Available online at www.sciencedirect.com
ScienceDirect
Journal of the European Ceramic Society 30 (2010) 3111–3116
www.elsevier.com/locate/jeurceramsoc

Thermal conductivities of YSZ/Al_2O_3 composites

Fan Yang, Xiaofeng Zhao, Ping Xiao *

Materials Science Centre, School of Materials, University of Manchester, M1 7HS, UK

Received 17 February 2010; received in revised form 15 June 2010; accepted 2 July 2010
Available online 25 July 2010

Abstract

The thermal conductivities/diffusivities of YSZ/Al_2O_3 composites have been investigated by a laser flash technique. The thermal conductivity of the composite increases with an increase in the Al_2O_3 volume fraction, and it can be fitted well to the Maxwell theoretical model. The consistency of the thermal conductivities of the composites with the predicted values indicates the absence of obvious interfacial thermal resistances in the composites. The negligible thermal resistance effect from the YSZ and Al_2O_3 grain boundaries is due to the much lower phonon mean free path compared with the grain size in the composite. The low Kapitza resistance of the YSZ/Al_2O_3 interface is discussed in terms of the "clean" and coherent nature of the YSZ/Al_2O_3 interface, together with the small difference between the elastic properties of YSZ and Al_2O_3.

Keywords: Thermal conductivity; Composites; Grain boundaries; Interfaces; Kapitza resistance

1. Introduction

A YSZ/Al_2O_3 composite is of both fundamental and practical interest. Because of the immiscibility of YSZ and Al_2O_3,[1] the YSZ/Al_2O_3 composite is of scientific importance in understanding the physical properties of a diphase system and ceramic/ceramic interfaces.[2] On the practical side, a YSZ/Al_2O_3 composite which combines the properties of the individual components has a wide range of applications. For example, a YSZ/Al_2O_3 composite has been proposed as an electrolyte for a planar Solid Oxide Fuel Cell (SOFC) because of its enhanced mechanical and thermal properties compared with conventional YSZ.[3] A YSZ/Al_2O_3 composite has the potential of being used as a thermal barrier coating (TBC) material because of its enhanced hardness, improved oxidation resistance for the substrate, and longer thermal cycling life than a conventional YSZ coating.[4] Therefore, an investigation of the thermal conductivity, which is an important physical property of a YSZ/Al_2O_3 composite, is necessary.

Another reason for studying the thermal conductivity of a YSZ/Al_2O_3 composite is to obtain the thermal properties of its interfaces. The existence of interfaces usually impedes the heat conduction by scattering the incident phonons and contributes to an interfacial thermal resistance (also known as the Kapitza resistance), which plays an important role in the thermal transport in nano-scale structures and devices.[5] The interfacial thermal resistance is also proposed as an important factor in selection of TBC candidate materials.[6] The Kapitza resistance of a YSZ/Al_2O_3 interface is also of special interest because during the high temperature service of a TBC, a thermally grown oxide (TGO) layer, which is mainly composed of α-Al_2O_3, forms at the substrate/coating interface.[7] Whether this YSZ/TGO (Al_2O_3) interface has influence on the thermal conductivity and how large this influence is, is an unsolved issue in the thermal conduction of TBCs. Consequently, an estimation of the Kapitza resistance of YSZ/Al_2O_3 interfaces is important.

The interfacial thermal resistance can be estimated by studying the thermal conductivity of the two-phase composite. Usually the effective thermal conductivity of a two-phase composite material without any interfacial thermal resistance can be predicted by the Maxwell theoretical model.[8] With the existence of a Kapitza resistance, the thermal conductivity of the composite will be lower than the value predicted by the Maxwell model. The interfacial thermal resistance can be estimated by the equation proposed by Hasselman and Johnson[9]

$$k_c = k_m \left[\frac{2((k_d/k_m) - (k_d/ah) - 1)v_d + ((k_d/k_m) + (2k_d/ah) + 2)}{(1 - (k_d/k_m) + (k_d/ah))v_d + ((k_d/k_m) + (2k_d/ah) + 2)} \right], \quad (1)$$

where k is the thermal conductivity; the subscripts c, m and d represent the composite, matrix and dispersed phase; a is the particle radius, h is the interfacial thermal conductance (i.e.,

* Corresponding author. Tel.: +44 161 3065941; fax: +44 161 3063586.
E-mail address: ping.xiao@manchester.ac.uk (P. Xiao).

0955-2219/$ – see front matter © 2010 Elsevier Ltd. All rights reserved.
doi:10.1016/j.jeurceramsoc.2010.07.007

Table 1
Measured densities, theoretical densities and relative densities of the YSZ/Al_2O_3 composites.

	Measured density (g/cm^3)	Theoretical density (g/cm^3)	Relative density (%)
YSZ	5.86 ± 0.03	5.96	98.3 ± 0.5
YSZ + 20% Al_2O_3	5.43 ± 0.03	5.56	97.7 ± 0.4
YSZ + 40% Al_2O_3	4.94 ± 0.03	5.17	95.6 ± 0.6
YSZ + 60% Al_2O_3	4.55 ± 0.02	4.77	95.4 ± 0.5
YSZ + 80% Al_2O_3	4.14 ± 0.02	4.38	94.6 ± 0.5
Al_2O_3	3.83 ± 0.02	3.98	96.5 ± 0.5

the reciprocal of the interfacial resistance) and ν_d is the volume fraction of the dispersed phase. When $h = \infty$, this indicates an absence of the interfacial thermal resistance, Eq. (1) is an expression of the Maxwell model.

Therefore in this paper, the thermal conductivity of a YSZ/Al_2O_3 composite was studied. The purpose of this study is not only to give an overall picture of the thermal conductivity of the composite, but also to promote an understanding of the Kapitza resistance of the YSZ/Al_2O_3 interfaces. The results may provide useful information for further application of the composite, as well as for further understanding of the thermal conduction in TBCs.

2. Experiments

8 mol.% YSZ powder (average particle size of 0.25 μm, PI-KEM, UK) and α-Al_2O_3 powder (average particle size 0.1–0.3 μm, PI-KEM, UK) were used as starting materials. Different compositions of YSZ/Al_2O_3 mixtures with 20, 40, 60, 80% (volume percentage) of Al_2O_3 were produced by a conventional solid mixing method. Appropriate amounts of YSZ and Al_2O_3 powders were weighed and then mixed by ball milling for 24 h in 2-propanol, using zirconia balls as the grinding media. The resulting mixtures were subsequently dried in air overnight, and then milled by mortar and pestle and passed through a 45 micro sieve. The final mixed powders were cold-pressed into cylindrical tablets under a uniaxial pressure of 100 MPa, and then sintered at 1500 °C for 4 h in air with a heating and cooling rate of 3 °C min^{-1}. Pure YSZ and Al_2O_3 tablets were also obtained by the same cold pressing and sintering procedures.

The densities of the sintered specimens were measured by Archimedes' method. The theoretical full densities of the YSZ/Al_2O_3 composites were obtained according to the rule of mixtures, i.e., $\rho = \nu_{YSZ}\rho_{YSZ} + \nu_{Al_2O_3}\rho_{Al_2O_3}$, where ν_{YSZ} and $\nu_{Al_2O_3}$ are the volume fractions of YSZ and Al_2O_3, and ρ_{YSZ} and $\rho_{Al_2O_3}$ are the theoretical densities of pure YSZ and Al_2O_3, which are 5.96 and 3.98 g/cm^3, respectively.[1,10] The measured densities, theoretical densities and the relative densities of the YSZ/Al_2O_3 composites are listed in Table 1.

The thermal diffusivity measurements were conducted with a laser flash system (Manchester, UK) from 50 °C up to 900 °C in an argon atmosphere. The specimens were in the form of disks, 1.5 mm thick and 11 mm in diameter. Before the measurements, the samples were mechanically ground to obtain coplanar surfaces. Both surfaces were coated with a thin layer of carbon using colloidal graphite (Agar Scientific Ltd., UK) to ensure complete and uniform absorption of the laser pulse. The samples were then dried to remove the remaining solvents. During the measurements, the front face of the samples was subjected to a short-duration heat pulse which was supplied by a neodymium-glass laser of 0.67 ms pulse duration. A liquid nitrogen cooled InSb infra-red detector was used to measure the temperature rise on the backside of the samples. Measurements were made at various chosen temperatures during the heating procedure. For each temperature, ten measurements were made to obtain the average value of the thermal diffusivity value.

The temperature dependence of the specific heat capacities of ZrO_2, Y_2O_3 and Al_2O_3 were obtained from Refs. 11–13, respectively. The specific heat of 8 mol.% YSZ was consequently calculated from the values of ZrO_2 and Y_2O_3 according to the Neumann-Kopp rule.[14] The calculated specific heat values for YSZ were compared with the reference values[15] and found to be consistent. The specific heat capacity values of the YSZ/Al_2O_3 composites at various temperatures were calculated from the rule of mixtures. The specific heat values are listed in Table 2.

The phase compositions of the YSZ/Al_2O_3 composites were identified by X-ray diffraction (XRD, Philips X'Pert) using Cu K_α radiation. The measurements were performed on the sample surfaces with a step scanning mode (step size of 0.05°) at a rate of 0.1° min^{-1}. The XRD patterns reveal that the composites consist of cubic YSZ and α-Al_2O_3, and confirm the very limited solid solubility between Al_2O_3 and YSZ.

Microstructures and the grain sizes of the YSZ/Al_2O_3 composites were observed by scanning electron microscope (SEM, Philips XL30). The microstructure of the YSZ/Al_2O_3 interface was observed by transmission electron microscopy (TEM). The sintered sample was ground to a thickness of approximately 100 μm and ultrasonically cut into discs of 3 mm diameter. The specimen thickness was further reduced to around 30 μm using a dimpling machine (Model D500, VCR Group, San Francisco, CA). After that, the specimen was cleaned in acetone and mounted onto a molybdenum grid and ion beam thinned using a Gatan (Oxford, UK) precision ion polishing system model 691 (PIPS^{TM}) operating at 4–6 kV. TEM observations were carried out using a FEI FEG TEM (Tecnai G2, Eindhoven, the Netherlands) operating at 300 kV.

3. Results and discussion

Fig. 1 shows the microstructure of the YSZ/Al_2O_3 composites. The white phase and the dark phase in the images

Table 2
The specific heat capacities of ZrO_2, Y_2O_3, Al_2O_3, 8 mol.% YSZ and the YSZ/Al_2O_3 composites at various temperatures.

Temperature (°C)	Specific heat capacity (J g^{-1} K^{-1})							
	ZrO_2[11]	Y_2O_3[12]	YSZ	Al_2O_3[13]	YSZ/Al_2O_3 composites with Al_2O_3 volume fractions of:			
					20%	40%	60%	80%
50	0.476	0.465	0.475	0.820	0.524	0.580	0.646	0.725
140	0.523	0.497	0.521	0.959	0.583	0.654	0.738	0.838
250	0.555	0.520	0.552	1.060	0.623	0.706	0.804	0.920
300	0.565	0.528	0.562	1.091	0.636	0.723	0.824	0.945
400	0.581	0.541	0.578	1.136	0.656	0.747	0.854	0.982
500	0.593	0.552	0.590	1.167	0.671	0.765	0.876	1.008
600	0.603	0.562	0.600	1.190	0.683	0.779	0.892	1.027
700	0.612	0.571	0.609	1.209	0.693	0.791	0.906	1.043
800	0.621	0.580	0.617	1.226	0.703	0.802	0.919	1.058
900	0.628	0.588	0.625	1.241	0.712	0.812	0.930	1.071

correspond to YSZ and Al_2O_3, respectively. It can be seen the minor phase disperses randomly in the major phase without large scale agglomerations.

The variations in the thermal diffusivity with temperature for the YSZ/Al_2O_3 composites are shown in Fig. 2. For all the compositions, the thermal diffusivity decreases monotonically with an increase in the temperature. The thermal conductivities (k) of the YSZ/Al_2O_3 composites were obtained from the heat capacity (C_p), density (ρ) and thermal diffusivity (α) values using the relationship:

$$k = \rho \cdot C_p \cdot \alpha, \quad (2)$$

and its dependence on the temperature is presented in the open symbols in Fig. 3. The thermal conductivity of YSZ has a temperature-independent value of around 2.1 W/(m K), which is in agreement with the reference value for 15 wt.% YSZ with a relative density of 98%.[15] For Al_2O_3, an obvious decrease in the thermal conductivity can be observed with an increase in

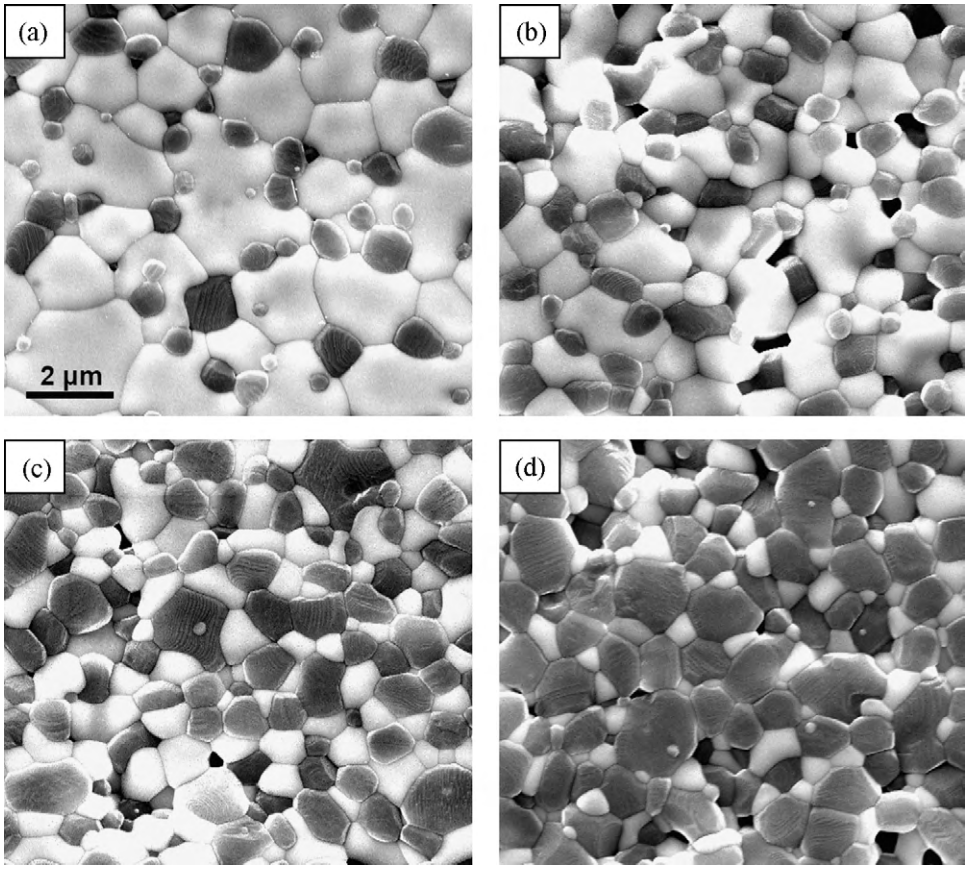

Fig. 1. Scanning electron micrographs of the YSZ/Al_2O_3 composites with different volume fraction of Al_2O_3: (a) 20%, (b) 40%, (c) 60% and (d) 80%. The white and dark phase corresponds to YSZ and Al_2O_3, respectively. The four images have the same scale bar.

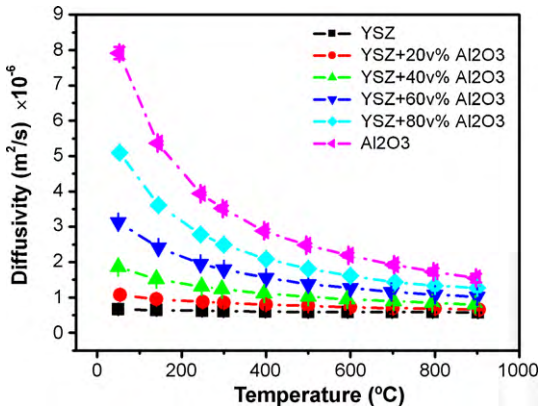

Fig. 2. Temperature dependence of the thermal diffusivities of the YSZ/Al_2O_3 composites.

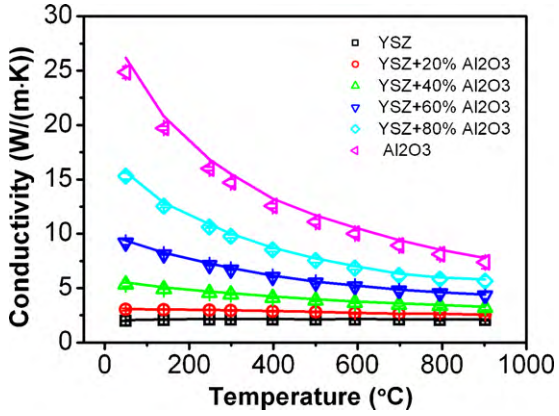

Fig. 3. Temperature dependence of the thermal conductivities of the YSZ/Al_2O_3 composites. The open symbols represent the measured values of the samples, while the solid lines represent the thermal conductivity of fully-dense samples calculated by Eqs. (3) and (4).

the temperature. The thermal conductivity of Al_2O_3 is close to, but slightly lower than the reported values in Ref. 16 possibly due to the slightly lower density in the present study. For the YSZ/Al_2O_3 composites, as may be expected, the thermal conductivity increases with an increase in the Al_2O_3 volume fraction because of the intrinsic thermal conductive property of Al_2O_3.

Before going on with further analysis, the effect of porosity on the thermal conductivity of the YSZ/Al_2O_3 composites should be eliminated to obtain the thermal conductivity values of the composites at full density. The YSZ/Al_2O_3 composites with pores can be treated as a "two-inclusion-phase composite",[17] and the thermal conductivity of the fully-dense composite (k_{cf}) can be evaluated with the following relationship[17]:

$$\frac{1}{k_{cp}} = \frac{k_{mf}}{k_{cf}k_{mp}} + \frac{(k_{mf} - k_{mp})(k_{cf} - k_{mf})}{3k_{mf}k_{cf}k_{mp}}, \quad (3)$$

where the subscripts cp, cf, mp and mf stand for composite with pores, fully-dense composite, matrix with pores and fully-dense matrix, respectively. The relationship between k_{mf} and k_{mp} is expressed as:

$$k_{mp} = \frac{1 - \nu_p}{1 + (\eta - 1)\nu_p} \cdot k_{mf}, \quad (4)$$

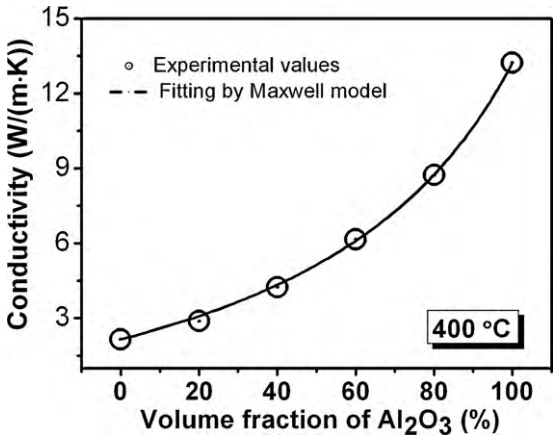

Fig. 4. Thermal conductivity of the YSZ/Al_2O_3 composites (corrected to zero porosity) as a function of the volume fraction of Al_2O_3 at 400 °C.

where ν_p is the volume fraction of the porosity and η is a parameter which is related to the pore shape. For spherical pores, η equals 1.5. For pure YSZ and Al_2O_3, the thermal conductivity at full density (k_{mf}) was evaluated with Eq. (4). When the volume fraction of Al_2O_3 is below 50%, YSZ is considered to be the matrix and therefore the calculated k_{mf} of YSZ was used in the subsequent calculations for the composite using Eq. (3). By contrast, when the volume fraction of Al_2O_3 exceeds 50%, Al_2O_3 is the matrix and the k_{mf} of Al_2O_3 was used for the subsequent calculations. The calculated thermal conductivities of fully-dense YSZ/Al_2O_3 composites at various temperatures are shown by the solid lines in Fig. 2. Only a slight increase of the thermal conductivity can be observed after correction.

Fig. 4 shows the thermal conductivity of the YSZ/Al_2O_3 composites as a function of the volume fraction of Al_2O_3, along with a fitting curve using the Maxwell model. It can be seen that the thermal conductivities predicted by the Maxwell model is in good agreement with the experimental values, which indicates the absence of an obvious interfacial thermal resistance in the YSZ/Al_2O_3 composite system, as discussed in the following paragraphs.

In the YSZ/Al_2O_3 composites, there are three types of interfaces: YSZ/YSZ (YSZ grain boundaries), Al_2O_3/Al_2O_3 (Al_2O_3 grain boundaries) and the YSZ/Al_2O_3 interfaces. The thermal resistance of the YSZ and the Al_2O_3 grain boundaries has been reported in the previous studies, i.e., Yang et al. studied the interfacial thermal resistance of nanocrystalline YSZ by measuring the grain-size-dependent thermal conductivity and obtained a value of 4.5×10^{-9} m^2 K/W for YSZ grain boundaries at room temperature[6]; Smith et al. investigated the thermal resistance of grain boundaries in Al_2O_3, and evaluated a value of 0.9–1.3 $\times 10^{-8}$ m^2 K/W in dense Al_2O_3.[18] However, the effect of grain boundaries can be observed only with the existence of a large number of interfaces (a small grain size of tens of nanometres) in YSZ. For example, Raghavan et al. found no obvious change of thermal conductivity in 5.8 wt.% YSZ when the grain size is larger than 100 nm.[15] For Al_2O_3, the early work by Charvat and Kingery[19] reported almost identical thermal conductivity of dense Al_2O_3 with grain sizes of 9 and 17 μm above 300 °C, indicating a negligible influence of grain boundaries. In

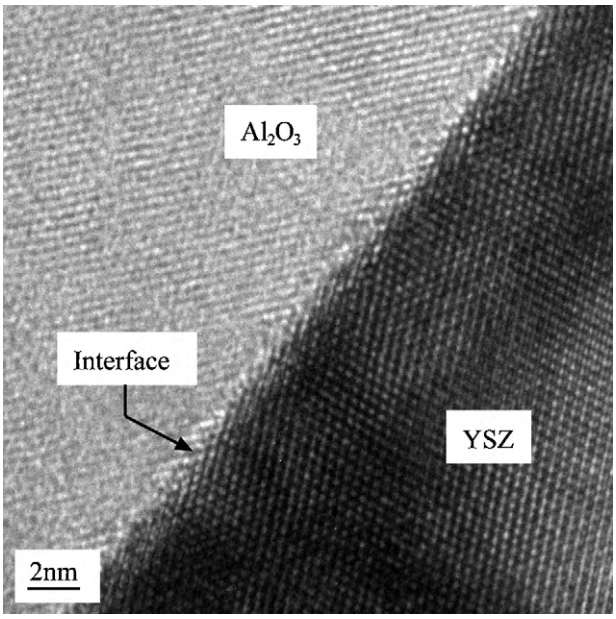

Fig. 5. High-resolution transmission electron microscopy (HRTEM) image of a YSZ/Al_2O_3 interface. The dark and bright regions represent YSZ and Al_2O_3 grains, respectively.

the present study, the average grain size of YSZ changes from ~10 μm in the pure YSZ to ~0.5 μm in the YSZ/Al_2O_3 composite with 80 v.% Al_2O_3, while the average grain size of Al_2O_3 varies from ~1 μm in the YSZ/Al_2O_3 composite with 20 v.% Al_2O_3 to ~5 μm in the pure Al_2O_3. It is known that the phonon mean free path in YSZ has a temperature-independent value of around 0.2 nm,[20] which is much smaller than the YSZ grain size in the composite. The phonon mean free path in Al_2O_3 is about 3 nm at room temperature,[19] and it decreases with increasing temperature following a T^{-1} law,[20] thus the phonon mean free path can be estimated to be 1.5 nm at 400 °C, which is more than 500 times smaller than the minimum Al_2O_3 grain size in the composite. Therefore, it can be concluded that neither the YSZ nor the Al_2O_3 grain boundaries have an influence on the thermal conductivity of the composites.

It is usually believed that an interface between two materials with different crystal structures and chemical natures has a larger thermal resistance than a grain boundary in a single-phase material.[18] The interfacial thermal resistance in a composite system can arise from the following aspects. First, the thermal expansion mismatch between the two components can cause imperfect mechanical contact[21,22] or interfacial separation.[23] However, this could not happen in the YSZ/Al_2O_3 composites since the thermal expansion coefficients of YSZ and Al_2O_3 have values close to each other, which are 8×10^{-6} and 10×10^{-6} °C^{-1}, respectively.[24] The YSZ/Al_2O_3 interface is adhesive and coherent without the existence of cracks, as can be seen in the TEM image in Fig. 5.

Second, dislocations and impurity segregations at the interface can act as scattering sites and contribute to the interfacial thermal resistance. However, the YSZ/Al_2O_3 interface is a "clean" interface: only atomic level lattice distortions can be observed without regions of large scale disorder, as also shown in Fig. 5. Also, impurity segregation is not observed at a YSZ/Al_2O_3 interface because of the "scavenging" effect of Al_2O_3.[25]

Another origin of the Kapitza resistance is the elastic discontinuity at the heterogeneous interface.[26] It is well known that the thermal conductivity of a material is expressed as

$$k = \frac{1}{3} C_V \upsilon L, \tag{5}$$

where C_V is the specific heat, υ is the phonon velocity and L is the phonon mean free path. The phonon velocity is correlated to the elastic property of the material by[27]:

$$\upsilon = 0.87\sqrt{\frac{E}{\rho}}, \tag{6}$$

where E and ρ are the Young's modulus and the density, respectively. When propagating across a heterogeneous interface, the phonons will be scattered to change their velocity, and consequently decrease the transmission probability of the phonons from one side to the other side. According to the diffuse mismatch model (DMM),[28] the phonon transmission probability is determined by the phonon velocity inside the two materials, as expressed by[28]:

$$\alpha = \frac{\sum_j \upsilon_{2,j}^{-2}}{\sum_j \upsilon_{2,j}^{-2} + \sum_j \upsilon_{1,j}^{-2}}, \tag{7}$$

where the subscripts "1", "2" and "j" refers to the side with the lower phonon velocity, the side with higher phonon velocity and the phonon mode (longitudinal or transverse), respectively. It can be seen from Eq. (7) that, a larger difference between the phonon velocity inside the two materials leads to a lower transmission probability. Since the interfacial thermal resistance is inversely proportional to the phonon transmission probability, it is expected that a large interfacial thermal resistance will exist between the two materials with significantly different Young's moduli. In the YSZ/Al_2O_3 composite system, the difference between the Young's moduli of YSZ and Al_2O_3 ($E_{Al_2O_3}/\rho_{Al_2O_3} \cdot \rho_{YSZ}/E_{YSZ} < 3$) is not large enough to have an obvious influence on the phonon transmission probability. Hasselman et al.[26] found the interfacial thermal barrier in a cordierite–diamond composite is less than 1.0×10^{-8} m^2 K/W at 400 °C, while the Young's modulus of diamond is almost ten times higher than that of cordierite (the density of diamond and cordierite is 3.51 and 2.52 g/cm^3, respectively). Therefore, it is possible that the thermal resistance of the YSZ/Al_2O_3 interface is even smaller than that value.

From the above analysis, it can be concluded that: (1) the negligible thermal resistance effect from the YSZ and Al_2O_3 grain boundaries is caused by the much lower phonon mean free path compared with the grain size in the composite; (2) the low Kapitza resistance is caused by the "clean" and coherent nature of the YSZ/Al_2O_3 interfaces, together with the small difference between the elastic properties of YSZ and Al_2O_3. Therefore, the thermal conductivity of the composite can be predicted well by the Maxwell model because of the absence of any interfacial thermal resistance.

Finally, there is a little remark on the good fitting of the experimental values with the Maxwell model in the YSZ/Al_2O_3 composites, especially when YSZ and Al_2O_3 have comparable volume fractions. Usually, Maxwell model requires dilute dispersions to avoid the interactions between the local temperature fields of neighbouring dispersions.[9] In YSZ/Al_2O_3 composites, the thermal conductivity values of YSZ and Al_2O_3 are not significantly different (for example, $k_{Al_2O_3}$ is only five times higher than k_{YSZ} at 400 °C). Therefore, the distortion of temperature gradient around the dispersed phase should be quite mild. In this case, the interaction of the temperature field between two inclusions is very small, and consequently extends the application range of Maxwell model. On the other hand, because of the small difference between the conductivity of YSZ and Al_2O_3, the temperature gradient is less dependent on the shape of the dispersed phase. As a result, although the shape of the minor phase is not perfect spherical in the composites, good fittings are still achieved between the experimental data and the Maxwell model.

4. Conclusion

The thermal conductivities/diffusivities of the YSZ/Al_2O_3 composites have been investigated by a laser flash technique from 50 °C to 900 °C. The thermal conductivity of the composites increases with an increase in the Al_2O_3 volume fraction, and it can be fitted well by the Maxwell theoretical model. The consistency of the thermal conductivity of the composite with the predicted values indicates the absence of interfacial thermal resistance in the composite. The negligible thermal resistance effect from the YSZ and Al_2O_3 grain boundaries is due to the low phonon mean free path compared with the grain size in the composite. The absence of a Kapitza resistance of the YSZ/Al_2O_3 interface is discussed from the "clean" and coherent nature of the YSZ/Al_2O_3 interface, together with the small difference between the elastic properties of YSZ and Al_2O_3. Although an exact value of the Kapitza resistance of the YSZ/Al_2O_3 interface was not obtained in this study, the results indicate the YSZ/Al_2O_3 interface is not thermally resistive.

Acknowledgements

The authors would like to acknowledge Dr. F. Azough for his kind help and useful suggestion on TEM sample preparation and Mr. A. Wallwork for his help on laser flash technique.

References

1. Feighery AJ, Irvine JTS. Effect of alumina additions upon electrical properties of 8 mol.% yttria-stabilized zirconia. *Solid State Ionics* 1999;**121**:209–16.
2. M' Peko JC, Spavieri Jr DL, da Silva CL, Fortulan CA, de Souza DPF, de Souza MF. Electrical properties of zirconia–alumina composites. *Solid State Ionics* 2003;**156**:59–69.
3. Mori M, Abe T, Itoh H, Yamamoto O, Takeda Y, Kawahara T. Cubic-stabilized zirconia and alumina composites as electrolytes in planar type solid oxide fuel cells. *Solid State Ionics* 1994;**74**:157–64.
4. Cao XQ, Vassen R, Stoever D. Ceramic materials for thermal barrier coatings. *J Eur Ceram Soc* 2004;**24**:1–10.
5. Reddy P, Castelino K, Majumdar A. Diffuse mismatch model of thermal boundary conductance using exact phonon dispersion. *Appl Phys Lett* 2005;**87**:211908.
6. Yang HS, Bai GR, Thompson LJ, Eastman JA. Interfacial thermal resistance in nanocrystalline yttria-stabilized zirconia. *Acta Mater* 2002;**50**:2309–17.
7. Evans AG, Mumm DR, Hutchinson JW, Meier GH, Pettit FS. Mechanisms controlling the durability of thermal barrier coatings. *Prog Mater Sci* 2001;**46**:505–53.
8. Maxwell JC. *A treatise on electricity and magnetism*. 3rd ed. New York: Dover Publications, Inc.; 1954. p. 57.
9. Hasselman DPH, Johnson LF. Effective thermal conductivity of composites with interfacial thermal barrier resistance. *J Comp Mater* 1987;**21**:508–15.
10. Shackelford JF, Alexander W. *CRC materials science and engineering handbook*. 3rd ed. Florida: CRC Press LLC; 2001. p. 81.
11. Coughlin JP, King EG. High-temperature heat contents of some zirconium-containing substances. *J Am Chem Soc* 1950;**72**:2262–5.
12. Landa YA, Polonskii YA, Glazachev BS, Milovidova TV. The enthalpy and specific heat of yttrium oxide at 1300–2100 °K. *Refract Ind Ceram* 1974;**15**:86–8.
13. Munro RG. Evaluated material properties for a sintered α-alumina. *J Am Ceram Soc* 1997;**80**:1919–28.
14. Kopp H. Investigations of the specific heat of solid bodies. *Phil Trans R Soc Lond* 1865;**155**:71–202.
15. Raghavan S, Wang H, Dinwiddie RB, Porter WD, Mayo MJ. The effect of grain size, porosity and yttria content on the thermal conductivity of nanocrystalline zirconia. *Scripta Mater* 1998;**39**:1119–25.
16. Barea R, Belmonte M, Osendi MI, Miranzo P. Thermal conductivity of Al_2O_3/SiC platelet composites. *J Eur Ceram Soc* 2003;**23**:1773–8.
17. Luo J, Stevens R, Taylor R. Thermal diffusivity/conductivity of magnesium oxide/silicon carbide composites. *J Am Ceram Soc* 1997;**80**:699–704.
18. Smith DS, Fayette S, Grandjean S, Martin C. Thermal resistance of grain boundaries in alumina ceramics and refractories. *J Am Ceram Soc* 2003;**86**:105–11.
19. Charvat FR, Kingery WD. Thermal conductivity: XIII, effect of microstructure on conductivity of single-phase ceramics. *J Am Ceram Soc* 1957;**40**:306–15.
20. Mevrel R, Laizet J, Azzopardi A, Leclercq B, Poulain M, Lavigne O, et al. Thermal diffusivity and conductivity of $Zr_{1-x}Y_xO_{2-x/2}$ ($x = 0$, 0.084 and 0.179) single crystals. *J Eur Ceram Soc* 2004;**24**:3081–9.
21. Bhatt H, Donaldson KY, Hasselman DPH, Bhatt RT. Role of interfacial thermal barrier in the effective thermal diffusivity/conductivity of SiC fiber-reinforced reaction-bonded silicon nitride. *J Am Ceram Soc* 1990;**73**:312–6.
22. Bhatt H, Donaldson KY, Hasselman DPH, Bhatt RT. Role of interfacial carbon layer in the thermal diffusivity/conductivity of SiC fiber-reinforced reaction-bonded silicon nitride matrix composites. *J Am Ceram Soc* 1992;**75**:334–40.
23. Ito YM, Rosenblatt M, Cheng LY, Lange FF, Evans AG. Cracking in particulate composites due to thermalmechanical stress. *Int J Fract* 1981;**17**:1183–91.
24. Cai PZ, Green DJ, Messing GL. Constrained densification of alumina/zirconia hybrid laminates, I: experimental observations of processing defects. *J Am Ceram Soc* 1997;**80**:1929–39.
25. Guo X, Waser R. Electrical properties of the grain boundaries of oxygen ion conductors: acceptor-doped zirconia and ceria. *Prog Mater Sci* 2006;**51**:151–210.
26. Hasselman DPH, Donaldson KY, Liu J, Gauckler LJ, Ownby PD. Thermal conductivity of a particulate-diamond-reinforced cordierite matrix composite. *J Am Ceram Soc* 1994;**77**:1757–60.
27. Clarke DR. Materials selection guidelines for low thermal conductivity thermal barrier coatings. *Surf Coat Technol* 2003;**163–164**:67–74.
28. Swartz ET, Pohl RO. Thermal boundary resistance. *Rev Mod Phys* 1989;**61**:605–68.